Russian Journal of Earth Sciences

Special Issue: "Data Science, Geoinformatics and Systems Analysis in Geosciences"

Enhanced Wintertime Convergence of Atmospheric and Oceanic Heat Transports in the Barents Sea Region under Present Climate Warming

M. M. Latonin[1], **I. L. Bashmachnikov**[1,2], **V. A. Semenov**[3,4]

[1]Nansen International Environmental and Remote Sensing Centre, Saint Petersburg, Russia
[2]Saint Petersburg State University, Saint Petersburg, Russia
[3]A. M. Obukhov Institute of Atmospheric Physics RAS, Moscow, Russia
[4]Institute of Geography RAS, Moscow, Russia
* **Correspondence to:** Mikhail M. Latonin, mikhail.latonin@niersc.spb.ru

Abstract: A distinctive feature of the Barents Sea climate system is a suggested positive feedback in the ocean–sea ice–atmosphere system that can enhance regional climate variations. The objective of this study is to assess the effectiveness of this positive feedback for the advective heat fluxes in the winter season using the ORAS4 ocean reanalysis and ERA5 atmospheric reanalysis data for the period 1959–2017. Based on the signs of the linear trends of the oceanic heat transport, two periods were identified for the analysis: 1959–1987 and 1987–2017. Composite maps of surface wind fields indicate an increase in the effectiveness of the positive feedback in the Barents Sea region during the present period relative to the previous one. This is manifested in the strengthening of the southern winds over the southeastern part of the sea in years with the maximum oceanic heat transport and in the weakening of the northern winds over the northwestern part of the sea in years with the minimum oceanic heat transport. The convergence of the atmospheric sensible heat transport over the Barents Sea has a maximum in the lower troposphere, 1000–900 hPa. An increasing synchronization of the convergence of atmospheric and oceanic heat transports in the Barents Sea region, derived in this study, contributes to an acceleration of the local warming.

Keywords: Barents Sea, advective heat fluxes, atmospheric and oceanic circulation, convergence, Arctic warming, climate feedbacks, reanalysis datasets.

Citation: Latonin, M. M., I. L. Bashmachnikov, and V. A. Semenov (2025), Enhanced Wintertime Convergence of Atmospheric and Oceanic Heat Transports in the Barents Sea Region under Present Climate Warming, *Russian Journal of Earth Sciences*, 25, ES2008, EDN: DRHLZX, https://doi.org/10.2205/2025ES000967

Research Article

Received: 15 November 2024
Accepted: 15 April 2025
Published: 23 May 2025

1. Introduction

The Barents Sea plays a crucial role in functioning of the Arctic climate system [*Bengtsson et al.*, 2004; *Smedsrud et al.*, 2013]. A unique geographical position of the Sea creates favorable conditions for the intense ocean–atmosphere coupling [*Eisbrenner et al.*, 2024], and the regional processes may even impact a global climate [*Semenov et al.*, 2010]. A warming rate in the Barents Sea area is the highest for the Arctic region [*Isaksen et al.*, 2022], and both atmospheric and oceanographic conditions are strongly impacted by the climate warming in this region [*Ingvaldsen et al.*, 2021; *Lind et al.*, 2018; *Przybylak et al.*, 2019]. An essential component of the heat budget of the Arctic and the Barents Sea are advective heat fluxes controlled by the atmospheric and oceanic circulation patterns [*Bashmachnikov et al.*, 2018; *Trenberth et al.*, 2001].

One of the important features of the regional climate dynamics in the Barents Sea is a positive feedback in the ocean–sea ice–atmosphere system [*Bengtsson et al.*, 2004; *Kalavichchi*

et al., 2019; 2021]. The increased oceanic heat influx into the Barents Sea is thought to contribute to the retreat of the sea ice edge. This in turn leads to the increased turbulent sensible and latent heat fluxes from the ocean to the atmosphere, which contributes to local cyclonic atmospheric vorticity. Such atmospheric circulation contributes to further enhancement of the convergence of oceanic and atmospheric heat transports in the region. This relatively local mechanism may actually impact a larger territory. For example, one of the leading explanations of the reasons of the early 20th century Arctic warming is related to this positive feedback loop [*Bengtsson et al.*, 2004]. If the inflow of the oceanic heat into the Barents Sea is restricted, the positive feedback in the Barents Sea might be reversed to act as a cooling mechanism leading at some conditions even to a shutdown of the oceanic inflow to the Sea [*Semenov et al.*, 2009].

This study focuses on the assessment of the effectiveness of positive feedback during the winter season in the ocean–sea ice–atmosphere system of the Barents Sea based on the ORAS4 and ERA5 reanalysis datasets for the period 1959–2017.

2. Data and methods

For the calculation of the oceanic heat transport, the seawater potential temperature and zonal current velocity were obtained from the ORAS4 reanalysis dataset [*Balmaseda et al.*, 2012]. For the calculation of the atmospheric sensible heat transport at isobaric surfaces 1000–100 hPa, the following variables were obtained from the ERA5 reanalysis dataset [*Hersbach et al.*, 2020]: air temperature, specific humidity, geopotential, zonal and meridional wind velocities. In addition, for the composite analysis, the mean surface sensible and latent heat fluxes, sea level atmospheric pressure, zonal and meridional components of the wind speed at 10 m were downloaded from the ERA5 archive. The analysis was performed for the extended winter season December–March. Figure 1 shows the study area with the sections used for the estimates of the advective heat fluxes in the ocean and atmosphere.

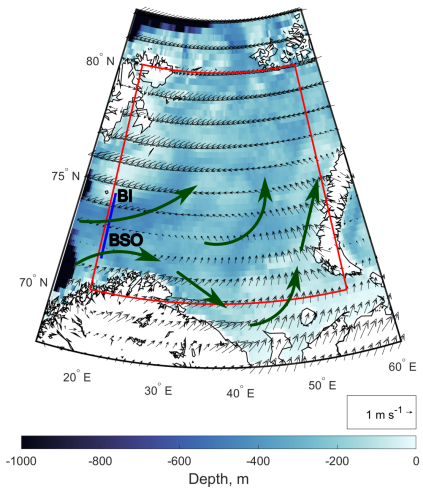

Figure 1. Study area with the sections for the calculation of the advective oceanic and atmospheric sensible heat fluxes. The blue line shows the section for the oceanic heat transport (20.5°E, 71.5°N–74.5°N), and the red lines show four sections for the atmospheric sensible heat transport (20°E, 70°N–80°N; 80°N, 20°E–55°E; 55°E, 70°N–80°N; 70°N, 20°E–55°E). Green arrows show schematic warm ocean currents from the North Atlantic entering the sea across the Barents Sea Opening (BSO); BI denotes Bear Island. Black arrows show mean wintertime surface wind directions at a height of 10 m over the period 1959–2017 based on the ERA5 reanalysis dataset. Bathymetry data are from the ETOPO 2022 15 Arc-Second Global Relief Model (https://www.ncei.noaa.gov/products/etopo-global-relief-model).

The oceanic heat flux (OHF) was calculated based on the monthly data as follows:

$$\mathrm{OHF}_{l,z,t(20.5°\mathrm{E})} = C_p\rho(\theta_{l,z,t} - \theta_{\mathrm{ref.}})U_{l,z,t},$$

where C_p is the typical specific heat capacity of seawater at constant pressure ($4000\,\mathrm{J\,kg^{-1}\,°C^{-1}}$), ρ is the typical seawater density ($1028\,\mathrm{kg\,m^{-3}}$), l is latitude, z is depth, t is time, θ is the monthly mean seawater potential temperature (°C), $\theta_{\mathrm{ref.}}$ is the reference temperature taken to be 0 °C, and U is the monthly mean eastward current velocity ($\mathrm{m\,s^{-1}}$). The reference temperature was set to 0 °C due to the established fact that it nearly corresponds to the outflow temperature of the cold waters leaving the Barents Sea [*Schauer et al.*, 2002].

The oceanic heat transport across the Barents Sea Opening was calculated as:

$$\mathrm{OHT} = \int_0^Z \int_{71.5°\mathrm{N}}^{74.5°\mathrm{N}} (\mathrm{OHF}_{l,z,t(20.5°\mathrm{E})})\mathrm{d}l\mathrm{d}z,$$

where integration over the latitude was carried out from 71.5°N to 74.5°N with a step $\mathrm{d}l = 1°$ (in meters), and over the depth, it was carried out from the surface to the bottom Z. Numerical integration was carried out by the trapezoidal method.

The atmospheric sensible heat fluxes (ASHF) were calculated based on the 6-hourly data as follows:

$$\begin{aligned}
\mathrm{ASHF}_{l,p,t(20°\mathrm{E})} &= C_p\rho T_{l,p,t(20°\mathrm{E})}U_{l,p,t(20°\mathrm{E})},\\
\mathrm{ASHF}_{l,p,t(80°\mathrm{N})} &= C_p\rho T_{l,p,t(80°\mathrm{N})}U_{l,p,t(80°\mathrm{N})},\\
\mathrm{ASHF}_{l,p,t(55°\mathrm{E})} &= C_p\rho T_{l,p,t(55°\mathrm{E})}U_{l,p,t(55°\mathrm{E})},\\
\mathrm{ASHF}_{l,p,t(70°\mathrm{N})} &= C_p\rho T_{l,p,t(70°\mathrm{N})}U_{l,p,t(70°\mathrm{N})},
\end{aligned}$$

where C_p is the typical specific heat capacity of air at constant pressure ($1005\,\mathrm{J\,kg^{-1}\,K^{-1}}$), ρ is the air density calculated according to (1), l is latitude or longitude, p is isobaric surface, t is time, T is the 6-hourly air temperature (K), Q is the 6-hourly specific humidity ($\mathrm{kg\,kg^{-1}}$), V is the 6-hourly northward wind velocity ($\mathrm{m\,s^{-1}}$) and U is the 6-hourly eastward wind velocity ($\mathrm{m\,s^{-1}}$).

$$\rho = \frac{P}{TR_d(1 + 0.61Q)}, \tag{1}$$

where P is atmospheric pressure (Pa), T is the 6-hourly air temperature (K), R_d is the specific gas constant for dry air ($287.04\,\mathrm{J\,kg^{-1}\,K^{-1}}$), Q is the 6-hourly specific humidity ($\mathrm{kg\,kg^{-1}}$). This method for the calculation of air density is taken from [*Brutsaert*, 1982].

The atmospheric sensible heat transports across the four sections displayed in Figure 1 were calculated as:

$$\begin{aligned}
\mathrm{ASHT}_{(20°\mathrm{E})} &= \int_{1000\mathrm{hPa}}^{900\mathrm{hPa}} \int_{70°\mathrm{N}}^{80°\mathrm{N}} (\mathrm{ASHF}_{l,p,t(20°\mathrm{E})})\mathrm{d}l\mathrm{d}p,\\
\mathrm{ASHT}_{(80°\mathrm{N})} &= \int_{1000\mathrm{hPa}}^{900\mathrm{hPa}} \int_{20°\mathrm{E}}^{55°\mathrm{E}} (\mathrm{ASHF}_{l,p,t(80°\mathrm{N})})\mathrm{d}l\mathrm{d}p,\\
\mathrm{ASHT}_{(55°\mathrm{E})} &= \int_{1000\mathrm{hPa}}^{900\mathrm{hPa}} \int_{70°\mathrm{N}}^{80°\mathrm{N}} (\mathrm{ASHF}_{l,p,t(55°\mathrm{E})})\mathrm{d}l\mathrm{d}p,\\
\mathrm{ASHT}_{(70°\mathrm{E})} &= \int_{1000\mathrm{hPa}}^{900\mathrm{hPa}} \int_{20°\mathrm{E}}^{55°\mathrm{E}} (\mathrm{ASHF}_{l,p,t(70°\mathrm{N})})\mathrm{d}l\mathrm{d}p,
\end{aligned}$$

where the horizonal integration step $\mathrm{d}l$ =0.25° expressed in meters, and the vertical integration step $\mathrm{d}p = 25\,\mathrm{hPa}$ expressed in meters according to the data on the geopotential heights (m) at each grid point corresponding to the isobaric surfaces. Numerical integration was carried out by the trapezoidal method. This method of estimation of the atmospheric heat

transport was used by [*Latonin et al.*, 2022]. The integration was performed for the layer 1000–900 hPa based on the results of the dominant directions of heat fluxes (see the section "Results").

The chosen sections for the calculation of the advective heat fluxes have been used in the previous studies [*Årthun et al.*, 2012; *Kalavichchi et al.*, 2021]. The oceanic section is also equivalent to the measure of the convergence of the oceanic heat transport into the Barents Sea [*Årthun et al.*, 2012]. For the atmospheric sections, as a measure of the convergence, the sum of the integral heat fluxes across four sections was used. Generally, the boundaries of the Barents Sea used in this study are commonplace [*Cai et al.*, 2022].

3. Results

Figure 2 shows the integral oceanic heat flux entering the Barents Sea. During 1959–2017, the mean wintertime oceanic heat transport across the Barents Sea Opening is 64 ± 4 TW. This quantity is in a good agreement with the simulated values of the oceanic heat transport across this section. For example, 59 TW was obtained in [*Årthun et al.*, 2012]. In another study, the oceanic heat transported by the North Cape Current across the western boundary of the Barents Sea to the south of the Bear Island was estimated to be 65 TW [*Bashmachnikov et al.*, 2018].

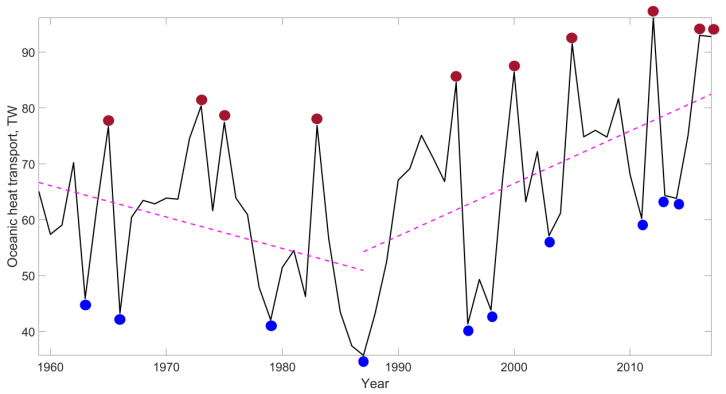

Figure 2. Wintertime oceanic heat transport across the western boundary of the Barents Sea. Dashed lines show linear trends for the periods 1959–1987 and 1987–2017. Red and blue circles mark the years with maxima and minima of the oceanic heat transport. The years with maxima and minima for the first period are: 1965, 1973, 1975, 1983 and 1963, 1966, 1979, 1987, respectively. The years with maxima and minima for the second period are: 1995, 2000, 2005, 2012, 2016, 2017 and 1996, 1998, 2003, 2011, 2013, 2014, respectively.

For further analysis, the time series was split into two parts: 1959–1987, when a statistically significant negative linear trend of −0.56 TW yr^{-1} was observed, and 1987–2017, when a statistically significant positive linear trend of 0.94 TW yr^{-1} was observed. Composite analysis was performed separately for the two periods, with averaging of four maxima and minima for the first period and of six extrema for the second period.

Figure 3 shows the mean ocean–atmosphere sensible and latent heat fluxes and their changes over two periods. The sum of two components was considered. It was reported in previous studies that the sensible heat flux strongly dominates over the latent heat flux, and the interannual variability of turbulent heat fluxes is the highest in the areas of strong sea ice reduction [*Årthun et al.*, 2010].

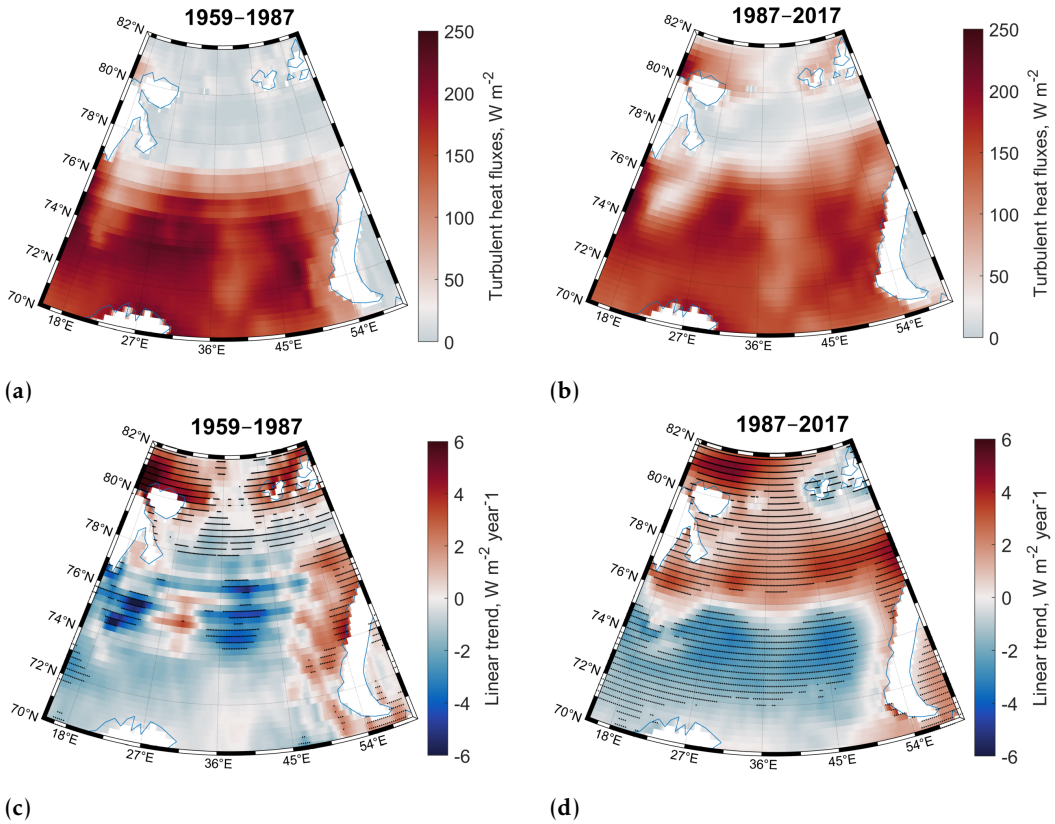

Figure 3. Mean values of total turbulent heat fluxes (a, b) for the first period (a) and for the second period (b) and linear trends of total turbulent heat fluxes (c, d) for the periods 1959–1987 (c) and 1987–2017 (d). Positive values on the maps (a) and (b) correspond to the direction of heat fluxes from the ocean to the atmosphere. Black dots on the maps (c) and (d) mark the areas of the statistically significant linear trends at the 5% significance level.

The structure of the obtained fields differs significantly between the two periods. These differences are related to the strong climate warming, which has begun in the 1980s. The area of the zones with the heat flux from the ocean to the atmosphere is higher for the modern period than for the previous one (Figure 3a, b). At the same time, the intensity of the heat flux ocean–atmosphere over the areas, where open water has always been observed, is lower in the modern period due to the increase in the air temperature and the decrease in the temperature difference between the ocean and the atmosphere. Figure 3d divides the sea practically into two parts: the northern part, in which the heat flux to the atmosphere increases due to the decrease in the concentration of sea ice, and the southern part, where the heat flux to the atmosphere decreases due to the decrease in the temperature contrast between water and air. It was found in [*Surkova et al.*, 2021] that anomalies in the turbulent heat fluxes and atmospheric pressure over the Barents Sea are coupled through changes in the North Atlantic Oscillation.

Composite maps of sea level atmospheric pressure anomalies for the maxima and minima in the oceanic heat transport are shown in Figure 4.

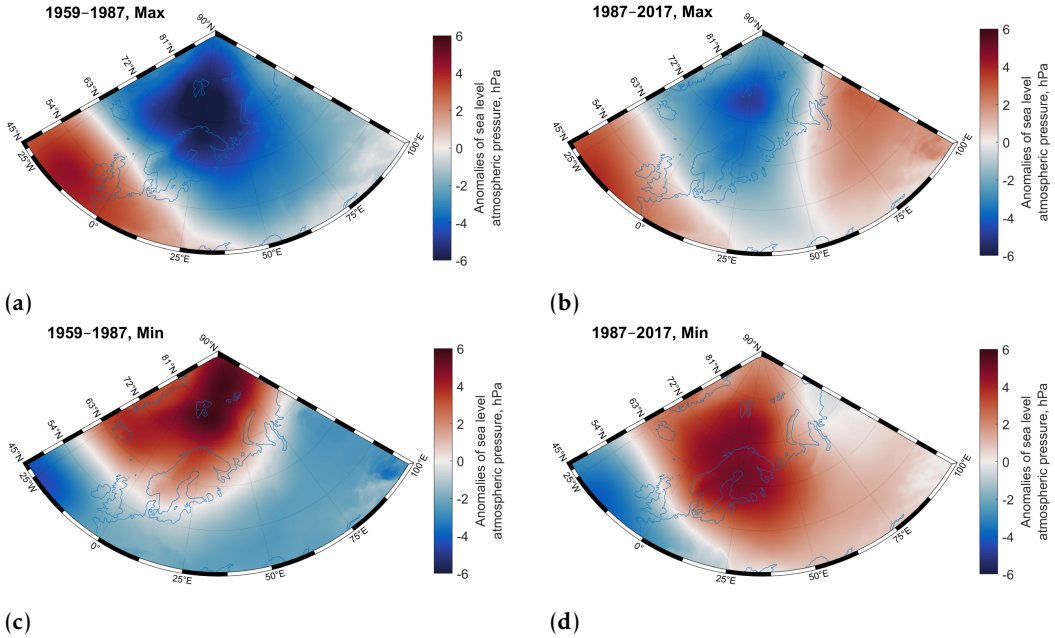

Figure 4. Anomalies of sea level atmospheric pressure relative to the periods 1959–1987 and 1987–2017 for the years with the maximum values of oceanic heat transport at the entrance to the Barents Sea (a, b) and for the years with the minimum values of oceanic heat transport at the entrance to the Barents Sea (c, d).

Negative pressure anomalies are observed over the Barents Sea and adjacent areas in the years with the maximum oceanic heat transport (Figure 4a, b), with the weaker anomaly for the modern period being compensated by a positive anomaly to the southeast of the sea (Figure 4b). The situation is opposite in the years with the minimum oceanic heat transport (Figure 4c, d). The negative pressure anomalies for the period 1987–2017 correspond to a more intense cyclonic atmospheric vorticity over the subpolar North Atlantic and the Barents Sea relative to the period 1959–1987 (Figure 5a, b). At the same time, the positive pressure anomalies for both periods correspond to the mostly cyclonic atmospheric vorticity over this region too; however, it is significantly weaker during 1959–1987 relative to 1987–2017 (Figure 5c, d). Thus, the cyclonic atmospheric vorticity over the Barents Sea has intensified in the present period. This pattern is consistent with the stronger oceanic heat release due to the sea ice reduction in the Barents Sea during 1987–2017 relative to 1959–1987 (Figure 3). It is known that generally, wind stress with cyclonic atmospheric vorticity contributes to an increase in the influx of oceanic heat into the Barents Sea.

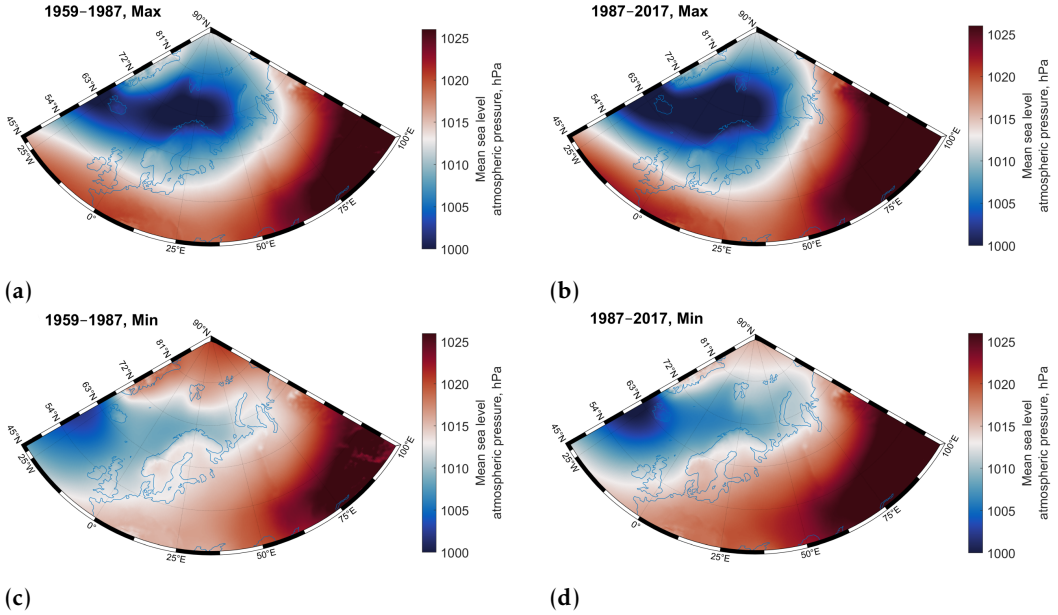

Figure 5. Mean sea level atmospheric pressure in the years with the maximum values of the oceanic heat transport at the entrance to the Barents Sea (a, b) and in the years with the minimum values of the oceanic heat transport at the entrance to the Barents Sea (c, d).

The mean wind fields corresponding to the maxima and minima of the oceanic heat transport are shown in Figure 6.

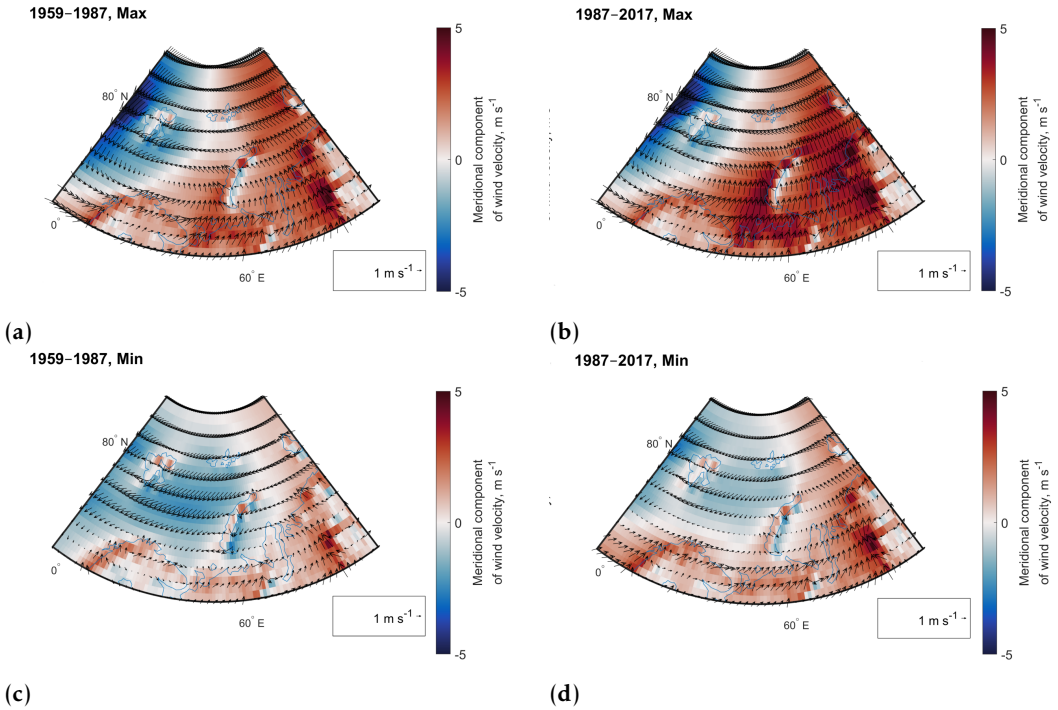

Figure 6. Mean wind velocity values (black arrows) at a height of 10 m in the years with the maximum values of the oceanic heat transport at the entrance to the Barents Sea (a, b) and in the years with the minimum values of the oceanic heat transport at the entrance to the Barents Sea (c, d). The colors show the values of the meridional component of the wind velocity; positive values correspond to the northward direction.

The composite maps in Figure 6 indicate an increase in the effectiveness of the positive feedback in the Barents Sea region in the modern period relative to the previous period. This is manifested in the strengthening of the southern winds over the southeastern part

of the sea in the years with the maximum oceanic heat transport (Figure 6a, b) and in the weakening of the northern winds over the northwestern part of the sea in the years with the minimum oceanic heat transport (Figure 6c, d). The relationship between the zonal oceanic heat transport and the meridional atmospheric heat transport is due to the fact that the cyclonic circulation is observed in the area of the western boundary of the Barents Sea (Figure 6a, b, d). These results are consistent with the previous findings by [*Kalavichchi et al.*, 2021], where an increase in the southern winds over the southeastern Barents Sea is accompanied by an increase of the oceanic heat transport across the Barents Sea Opening during the present period of climate warming.

Figure 7 shows the time-altitude diagrams for the atmospheric sensible heat fluxes.

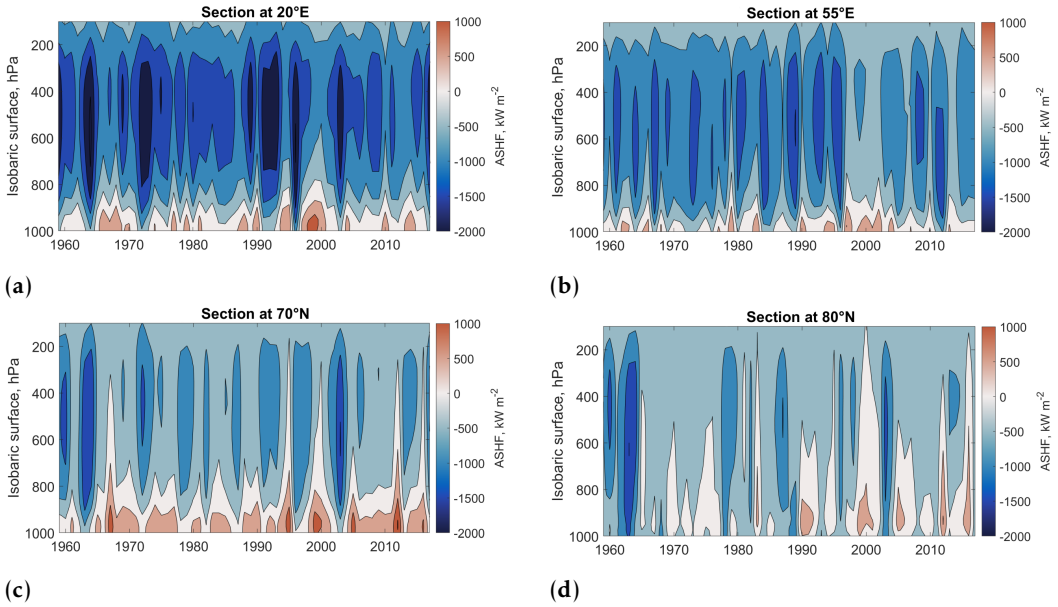

Figure 7. Vertical sections of atmospheric sensible heat flux (ASHF, kW m^{-2}). (a) Mean wintertime sensible heat flux across the section at 20°E, (b) Mean wintertime sensible heat flux across the section at 55°E, (c) Mean wintertime sensible heat flux across the section at 70°N, (d) Mean wintertime sensible heat flux across the section at 80°N. Positive values indicate heat flux to the west (a, b) and to the north (c, d).

According to the obtained vertical profiles, atmospheric sensible heat fluxes are directed predominantly to the west and north in the layer of the lower troposphere 1000–900 hPa, while in the higher levels, the direction changes to the opposite. At the same time, the intensity of fluxes is higher at the western and southern boundaries (Figure 7a, c) than at the eastern and northern boundaries (Figure 7b, d). Thus, only atmospheric circulation in the lower troposphere is directly involved in the emergence of the studied positive feedback. Therefore, integral heat fluxes in the 1000–900 hPa layer were then calculated for each atmospheric section.

The convergences of the oceanic and atmospheric heat transports are shown in Figure 8. The mean atmospheric heat convergence over the studied period is 401 ± 223 TW. The uncertainty is high due to very strong variability. The mean wintertime atmospheric heat transport convergence of 405 TW based on the ERA-Interim reanalysis dataset was reported in [*Kalavichchi et al.*, 2019]. This quantity is very close to 401 TW found in the present study. Thus, the atmospheric heat transport convergence strongly dominates over the oceanic heat transport convergence, which is only 64 TW.

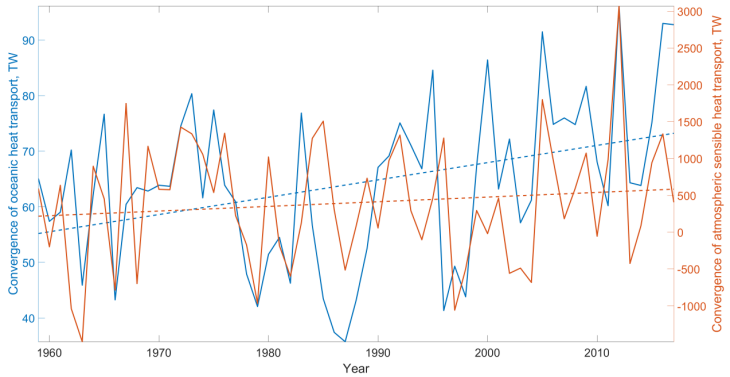

Figure 8. Convergence of oceanic and atmospheric heat transports in the Barents Sea region. 1 TW = 10^{12} W. Dashed lines show linear trends.

According to Figure 8, the correlation coefficient for the entire period 1959–2017 is 0.44. At the same time, for the period 1959–1987, the correlation is only 0.39, and for the period 1987–2017 it increases to 0.54. All correlations are statistically significant and reach a maximum with a zero time lag. The maximum correlation coefficient of 0.76 is achieved for the period 2003–2017. Therefore, one can conclude that over the modern period, the efficiency of positive feedback in the Barents Sea area has increased. This result indicates an increasing synchronization of the convergence of oceanic and atmospheric heat transports in the area of the Barents Sea, which contributes to an amplification of the local warming.

4. Conclusions

The results of the present study point out that climate warming contributes to the emergence of the effectiveness of the positive feedback in the Barents Sea region, which leads to a stronger warming in the area. The growing coherence of the atmospheric heat convergence with the growing oceanic heat transport into the sea contributes to the accelerated warming of the atmosphere over the Barents Sea compared to the rest of the Arctic Ocean.

The atmospheric circulation has become more meridional during the present period of climate warming, which is supported by the previous studies [*Francis et al.*, 2012]. This feature is related to the changes in the large-scale atmospheric circulation, with a growing role of the Siberian High [*Inoue et al.*, 2012; *Kalavichchi et al.*, 2021]. These processes affect the positive feedback in the Barents Sea area. Thus, although the Barents Sea has a unique climate system with the local feedback, the processes here are strongly coupled to the large-scale atmospheric circulation.

In turn, the accelerated sea ice retreat and corresponding wintertime increase of the sensible heat flux were suggested to lead to more frequent anticyclonic blocking events, which results in colder winters in Europe in the beginning of the 21th century [*Petoukhov et al.*, 2010; *Semenov et al.*, 2015].

Acknowledgments. This study was funded by the Russian Science Foundation (RSF), grant number 23-77-01046 (https://rscf.ru/en/project/23-77-01046/). M. M. L. would like to thank Alexander P. Makshtas for the valuable discussion on the methodology and advice.

References

Årthun M., Schrum C. Ocean surface heat flux variability in the Barents Sea // Journal of Marine Systems. — 2010. — Vol. 83, no. 1/2. — P. 88–98. — DOI: 10.1016/j.jmarsys.2010.07.003.

Årthun M., Eldevik T., Smedsrud L. H., et al. Quantifying the Influence of Atlantic Heat on Barents Sea Ice Variability and Retreat // Journal of Climate. — 2012. — Vol. 25, no. 13. — P. 4736–4743. — DOI: 10.1175/jcli-d-11-00466.1.

Balmaseda M. A., Mogensen K., Weaver A. T. Evaluation of the ECMWF ocean reanalysis system ORAS4 // Quarterly Journal of the Royal Meteorological Society. — 2012. — Vol. 139, no. 674. — P. 1132–1161. — DOI: 10.1002/qj.2063.

Bashmachnikov I. L., Yurova A. Y., Bobylev L. P., et al. Seasonal and Interannual Variations of Heat Fluxes in the Barents Sea Region // Izvestiya, Atmospheric and Oceanic Physics. — 2018. — Vol. 54, no. 2. — P. 213–222. — DOI: 10.1134/s0001433818020032.

Bengtsson L., Semenov V. A., Johannessen O. M. The Early Twentieth-Century Warming in the Arctic - A Possible Mechanism // Journal of Climate. — 2004. — Vol. 17, no. 20. — P. 4045–4057. — DOI: 10.1175/1520-0442(2004)017<4045:tetwit>2.0.co;2.

Brutsaert W. Evaporation into the Atmosphere. — Springer Netherlands, 1982. — DOI: 10.1007/978-94-017-1497-6.

Cai Z., You Q., Chen H. W., et al. Amplified wintertime Barents Sea warming linked to intensified Barents oscillation // Environmental Research Letters. — 2022. — Vol. 17, no. 4. — DOI: 10.1088/1748-9326/ac5bb3.

Eisbrenner E., Chafik L., Åslund O., et al. Interplay of atmosphere and ocean amplifies summer marine extremes in the Barents Sea at different timescales // Communications Earth & Environment. — 2024. — Vol. 5, no. 1. — DOI: 10.1038/s43247-024-01610-5.

Francis J. A., Vavrus S. J. Evidence linking Arctic amplification to extreme weather in mid-latitudes // Geophysical Research Letters. — 2012. — Vol. 39, no. 6. — DOI: 10.1029/2012gl051000.

Hersbach H., Bell B., Berrisford P., et al. The ERA5 global reanalysis // Quarterly Journal of the Royal Meteorological Society. — 2020. — Vol. 146, no. 730. — P. 1999–2049. — DOI: 10.1002/qj.3803.

Ingvaldsen R. B., Assmann K. M., Primicerio R., et al. Physical manifestations and ecological implications of Arctic Atlantification // Nature Reviews Earth & Environment. — 2021. — Vol. 2, no. 12. — P. 874–889. — DOI: 10.1038/s43017-021-00228-x.

Inoue J., Hori M. E., Takaya K. The Role of Barents Sea Ice in the Wintertime Cyclone Track and Emergence of a Warm-Arctic Cold-Siberian Anomaly // Journal of Climate. — 2012. — Vol. 25, no. 7. — P. 2561–2568. — DOI: 10.1175/jcli-d-11-00449.1.

Isaksen K., Nordli Ø., Ivanov B., et al. Exceptional warming over the Barents area // Scientific Reports. — 2022. — Vol. 12, no. 1. — DOI: 10.1038/s41598-022-13568-5.

Kalavichchi K. A., Bashmachnikov I. L. Mechanism of a Positive Feedback in Long-Term Variations of the Convergence of Oceanic and Atmospheric Heat Fluxes and of the Ice Cover in the Barents Sea // Izvestiya, Atmospheric and Oceanic Physics. — 2019. — Vol. 55, no. 6. — P. 640–649. — DOI: 10.1134/s0001433819060173.

Kalavichchi K. A., Bashmachnikov I. L. Ocean–Atmosphere Interactions in the Barents Sea from Reanalyses Data // Izvestiya, Atmospheric and Oceanic Physics. — 2021. — Vol. 57, no. 2. — P. 159–169. — DOI: 10.1134/s0001433821020067.

Latonin M. M., Bobylev L. P., Bashmachnikov I. L., et al. Dipole pattern of meridional atmospheric internal energy transport across the Arctic gate // Scientific Reports. — 2022. — Vol. 12, no. 1. — DOI: 10.1038/s41598-022-06371-9.

Lind S., Ingvaldsen R. B., Furevik T. Arctic warming hotspot in the northern Barents Sea linked to declining sea-ice import // Nature Climate Change. — 2018. — Vol. 8, no. 7. — P. 634–639. — DOI: 10.1038/s41558-018-0205-y.

Petoukhov V., Semenov V. A. A link between reduced Barents-Kara sea ice and cold winter extremes over northern continents // Journal of Geophysical Research: Atmospheres. — 2010. — Vol. 115, no. D21. — DOI: 10.1029/2009jd013568.

Przybylak R., Wyszyński P. Air temperature changes in the Arctic in the period 1951–2015 in the light of observational and reanalysis data // Theoretical and Applied Climatology. — 2019. — Vol. 139, no. 1/2. — P. 75–94. — DOI: 10.1007/s00704-019-02952-3.

Schauer U., Loeng H., Rudels B., et al. Atlantic Water flow through the Barents and Kara Seas // Deep Sea Research Part I: Oceanographic Research Papers. — 2002. — Vol. 49, no. 12. — P. 2281–2298. — DOI: 10.1016/s0967-0637(02)00125-5.

Semenov V. A., Park W., Latif M. Barents Sea inflow shutdown: A new mechanism for rapid climate changes // Geophysical Research Letters. — 2009. — Vol. 36, no. 14. — DOI: 10.1029/2009gl038911.

Semenov V. A., Latif M., Dommenget D., et al. The Impact of North Atlantic–Arctic Multidecadal Variability on Northern Hemisphere Surface Air Temperature // Journal of Climate. — 2010. — Vol. 23, no. 21. — P. 5668–5677. — DOI: 10.1175/2010jcli3347.1.

Semenov V. A., *Latif M.* Nonlinear winter atmospheric circulation response to Arctic sea ice concentration anomalies for different periods during 1966–2012 // Environmental Research Letters. — 2015. — Vol. 10, no. 5. — DOI: 10.1088/1748-9326/10/5/054020.

Smedsrud L. H., *Esau I.*, *Ingvaldsen R. B.*, *et al.* The Role of the Barents Sea in the Arctic Climate System // Reviews of Geophysics. — 2013. — Vol. 51, no. 3. — P. 415–449. — DOI: 10.1002/rog.20017.

Surkova G. V., *Romanenko V. A.* Climate change and heat exchange between atmosphere and ocean in the Arctic based on data from the Barents and the Kara sea // Arctic and Antarctic Research. — 2021. — Vol. 67, no. 3. — P. 280–292. — DOI: 10.30758/0555-2648-2021-67-3-280-292.

Trenberth K. E., *Caron J. M.* Estimates of Meridional Atmosphere and Ocean Heat Transports // Journal of Climate. — 2001. — Vol. 14, no. 16. — P. 3433–3443. — DOI: 10.1175/1520-0442(2001)014<3433:eomaao>2.0.co;2.